

## IMAGE-BASED DIAGNOSTICS OF THE PLASMA PRODUCED IN 1 PW LASER EXPERIMENTS

A. MĂGUREANU<sup>1,2</sup>, S. BĂLĂȘCUȚĂ<sup>1</sup>, P. GHENUCHE<sup>1</sup>, M. O. CERNĂIANU<sup>1</sup>, L. TUDOR<sup>1</sup>, V. NASTASA<sup>1</sup>, D.G. GHIȚĂ<sup>1</sup>, B. DIACONESCU<sup>1</sup>, D. DORIA<sup>1</sup>, C.M TICOȘ<sup>1,2</sup>

<sup>1</sup>Extreme Light Infrastructure - Nuclear Physics, "Horia Hulubei" National Institute for R&D in Physics and Nuclear Engineering, 30 Reactorului Street, 077125 Magurele, Romania

<sup>2</sup>Engineering and Applications of Lasers and Accelerators Doctoral School (SDIALA), National University of Science and Technology Politehnica of Bucharest, Bucharest, Romania  
E-mail: alexandru.magureanu@eli-np.ro

*Received*

Plasma imaging diagnostics are essential tools for gaining insight into the laser-driven plasma dynamics in experiments with high-power lasers. This study details the design and implementation of an imaging system based on shadowgraphy measurements, integrated with wavefront sensor measurements, during the experiments conducted in the commissioning phase of the Extreme Light Infrastructure - Nuclear Physics (ELI-NP) facility. The shadowgraphy system was employed to capture detailed images of the plasma plume generated by the 1PW laser pulses directed at both solid and gaseous targets. The wavefront sensor measurements reveal the phase shift of the wavefront of the probe beam as it traverses the plasma channel formed by the laser beam focused into a gas cell. Our findings highlight the importance of these imaging diagnostic techniques in evaluating the complex dynamics of laser-plasma interaction for the advancement of laser-driven particle acceleration.

*Key words:* high power laser, plasma imaging, shadowgraphy

### 1. INTRODUCTION

Advancements in ultra-short, high-power laser experiments are unlocking new opportunities for particle acceleration and radiation generation, paving the way for the rapidly evolving field of nuclear photonics [1,2,3,4]. The increasing complexity of experiments with multi-PW lasers underlines the growing need for accurate plasma diagnostics [5,6]. The region where the high-intensity laser interacts with the target serves as the primary source of the physical phenomena under investigation, whether a solid foil is used for ion acceleration or a gas jet for electron acceleration. Laser-plasma interactions need to be investigated with dedicated diagnostics, some of them being able to resolve very fast phenomena with duration of a few picoseconds or less.

Imaging of the plasma produced by ultrashort, high peak-power laser pulses focused into either a gas or onto a solid target serves as an essential diagnostic

technique in experiments. Particularly, the shadowgraphy approach is a robust and straightforward imaging diagnostic technique that uses a probe beam extracted from the main laser beam using a pick-off mirror to illuminate the plasma channel formed by a high-intensity laser pulse inside a gas jet or cell [7]. Illuminating the gas cell from the side produces a shadow image of the interaction, which is then recorded by a CCD camera. This technique can be enhanced by employing a wavefront sensor camera equipped with a specialized CCD to measure the phase gradient of the beam in the recorded image, allowing for the calculation of the density of the gas or of the plasma when the laser ionizes the gas [8]. During thin foil irradiation experiments, the probe beam captures the shadow of the rapidly expanding plasma plume created by the focused laser as it is ionizing the solid target [5-11].

## 2. EXPERIMENTAL SET-UP

Accurate alignment of the pulsed main beam with the probe beam is essential for the imaging process, requiring precise spatial and temporal synchronisation between the two beams. In the experimental configuration at the 1 PW laser facility of ELI-NP [10], the probe beam was reflected by a 1-inch dielectric elliptical pick-off mirror positioned at the periphery of the main beam cross-section. The main beam, delivered by a Ti:sapphire laser, had a diameter of approximately 200 mm, a peak power of up to 1 PW, a duration from 25 to 30 fs, and a central wavelength of 800 nm [12]. At the pick-off mirror location, the energy of the 25 mm diameter probe beam can be approximated by the following formula when considering a flat-top laser beam profile:

$$E_{probe} = E_{main} \left( \frac{S_{probe}}{S_{main}} \right) \quad (1)$$

where  $E_{probe} \approx 1.56 \times 10^{-2} E_{main}$ , and  $S_{probe}$  and  $S_{main}$  are the areas of the cross-sections of the probe and main laser beams, respectively. As an example, for  $E_{main} = 20 J$  the probe pulse energy is  $E_{probe} \approx 300 mJ$ . This is particularly important for knowing the fluence of the probe beam which needs to be correlated with the damage threshold of the optics inserted in the path of the beam. For a femtosecond-optimized silver-coated mirror typically used in the setup, the damage threshold is about 380-390 mJ/cm<sup>2</sup> for single-shot pulses with duration ranging from 40 to 52 fs [13,14]. In our case, the fluence was below this level at about 60 mJ/cm<sup>2</sup>.

The pulsed probe beam, having the same duration as the main laser pulse, is time-delayed by reflections on the multiple mirrors of a delay line provided with a motorized stage with 2  $\mu$ m displacement step corresponding to 6.6 fs step delay. The travel range is 20 cm providing flexibility for adjusting the optical path length,

enabling imaging of the interaction across various timescales. This includes capturing events a few picoseconds prior to the main pulse's interaction with the gas target, as well as, subsequent plasma evolution. Figure 1. illustrates the imaging systems employed in the current setup.

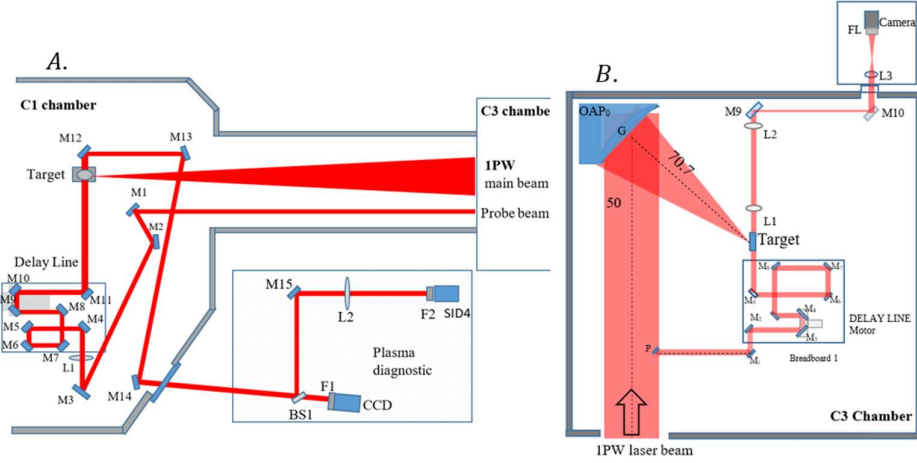


Fig. 1 – A. Sketch of the simplified imaging system for a gas jet experiment for electron acceleration, which incorporates the delay line, a CCD camera for shadowgraphy, and the wavefront sensor SID4 (M1 – M13 – Reflecting mirrors, L1,L2 - Lenses for imaging the interaction, BS1 – Beam splitter, F1,F2 – Filters for the camera). B. Sketch of the imaging system for a solid target experiment for protons acceleration that incorporates the delay line and the shadowgraphy system (OAP – Off-Axis Parabolic Mirror, for focusing the main beam in the target, M1 – M10 – Reflecting mirrors, L1-L3 - Lenses for imaging the interaction, FL – Filter for the camera)

Figure 1A illustrates the imaging diagnostic system which incorporates the delay line, the SID4 camera and a wavefront sensor designed to perform Quadri-Wave Lateral Shearing Interferometry (QWLSI) for generating phase maps of plasma images. This interferometric method measures the phase gradient along one direction by exploiting the interference of two identical, but tilted wavefronts derived from the same incident wavefront. The approach was extended to multi-wave interferometry [9], enabling the measurement of multiple gradients to reconstruct the complete 2D phase field. In QWLSI, four replicas of the wavefront are produced using a specialized two-dimensional diffraction grating integrated in front of the camera sensor [14]. By integrating the phase gradients along two perpendicular axes, both the intensity and phase of the wavefront are determined [15]. The measured phase drift in the image of the interference pattern is proportional to the plasma electron density and indicates the difference between the refractive index of the plasma and the refractive index of the vacuum. Assuming  $d$  is the distance in the

plasma through which the laser pulse is propagating along the  $Z$ -axis, the resulting phase shift of the pulse wavefront can be expressed as follows:

$$\varnothing = \int_0^d \mathbf{k}_p \cdot d\mathbf{z} = \int_0^d \frac{N(z)\omega}{c} \cdot d\mathbf{z} \quad (2)$$

where  $\mathbf{k}_p$  represents wavefront vector of the laser beam,  $N(\mathbf{z})$  represents the local refractive index of the plasma,  $\omega$  represents the laser frequency, and  $c$  is the speed of light. A reference phase image is first recorded by directing the laser pulse through a vacuum without the gas target. Then, a second laser pulse is transmitted through the ionized gas target. The phase differences between the two laser pulses are described by equation (3), where  $N_0 = 1$  is the index of refraction for vacuum:

$$\Delta\varnothing = \int_0^d (N_0 - N(z)) \omega/c \cdot d\mathbf{z} \quad (3)$$

Considering the plasma electron density, the critical plasma density  $n_{cr} = \frac{\epsilon_0 \cdot m_e \cdot \omega^2}{e^2}$  and the plasma frequency  $\omega_p^2 = (n_e e^2)/(m_e \cdot \epsilon_0)$ , the laser frequency is given by  $\omega^2 = (n_{cr} e^2)/(m_e \cdot \epsilon_0)$ . The refractive index  $N(\mathbf{z})$  is linked to the density of the plasma:  $N^2 = 1 - n_e/n_{cr}$ . For the electron density of plasma much smaller than the critical density, one can approximate  $N \approx 1 - n_e/(2n_{cr})$  such that the phase difference is given by:

$$\Delta\varnothing \approx \int_0^d \frac{n_e(z) \omega}{2n_{cr} c} d\mathbf{z} = \frac{\omega \cdot d}{2 \cdot c} \cdot \frac{\bar{n}_e}{n_{cr}} = \frac{\pi \cdot d}{\lambda} \cdot \frac{\bar{n}_e}{n_{cr}} \quad (4)$$

In the above equation  $\bar{n}_e = \int_0^d n_e(z) dz / d$  is the average plasma density along the probed plasma column of thickness  $d$ . Equation (4) allows the average density to be estimated along a direction parallel to the probe axis. The SID4 wavefront sensor system integrates a standard camera and a two-dimensional diffraction grating that produces on the camera's sensor an interferogram. From this interferogram, both the profile and the intensity and wavefront profile  $\mathbf{W}(\mathbf{x}, \mathbf{y})$  of the light beam are determined. When the beam traverses the plasma, the sensor captures a phase shift map  $\Delta\varnothing(\mathbf{x}, \mathbf{y})$  in the image plane. To retrieve the plasma density and the refractive index, an algorithm employing the inverse Abel transform can be applied if the geometry has a cylindrical symmetry [16].

### 3. RESULTS

Plasma imaging diagnostics were employed during the experimental campaign for electron acceleration in the interaction chamber C1 of the 1 PW, E5 experimental area. The laser ionized the gas, forming a plasma channel, and the plasma density was estimated from an image recorded by the SID4 Phasics wavefront sensor camera. In this plasma channel image, a Region of Interest (ROI) was selected using the software package provided by Phasics. Figure 2 shows a map of the density of plasma in 2D, plotted against both the axial (along the laser) and transverse directions relative to the plasma channel. The obtained values for the electron densities were  $n_e \sim 2 - 4 \times 10^{18} \text{ cm}^{-3}$ , in line with measurements reported elsewhere [7]

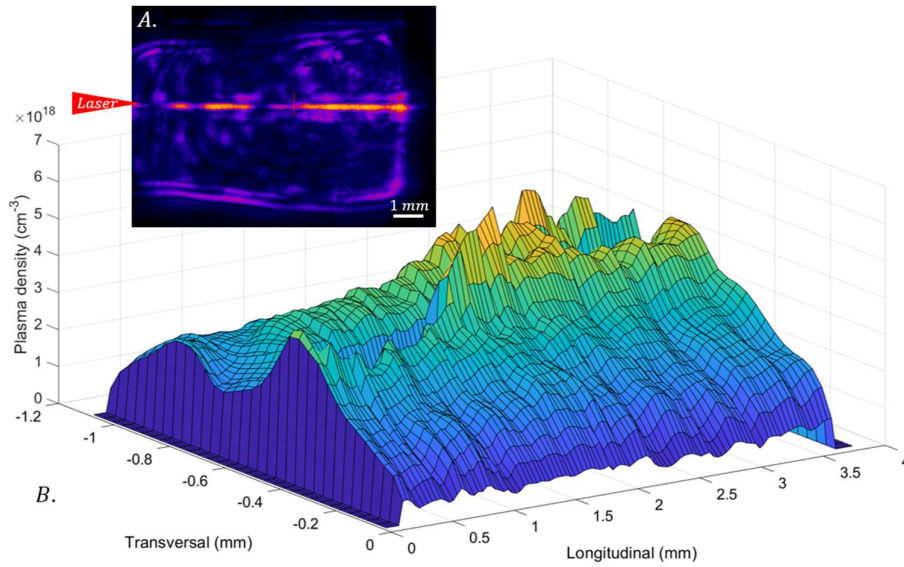


Fig. 2. A. Shadowgraphy images with a selection of the ROI used for the plasma channel, B. Electron density map in 2D in the viewing plane (x,y) with Ox being the axial direction along the laser and Oy the transverse direction

Figure 3 shows the shadowgraphy image taken with the EDGE 5.5 MP PCO camera, both before and after the interaction of the main laser pulse with the gas target. A 1 cm long 3D printed gas cell was used for this setup. One can clearly see the plasma channel which has a width of  $\approx 200\text{-}300 \mu\text{m}$  and a length of 1 cm.

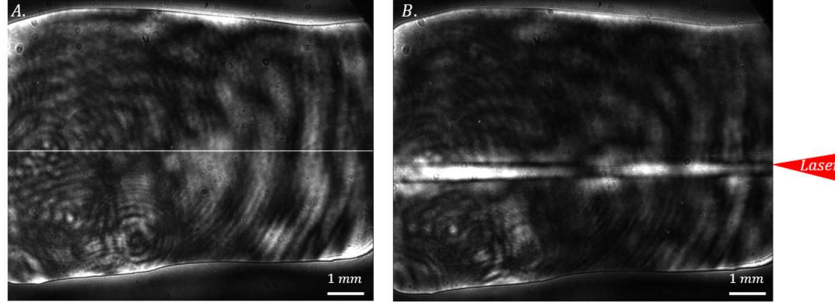


Fig. 3. A) Shadowgraphy from the side view photos of the cell filled with Ar gas during interaction with the laser: A. Image of the gas cell before the laser-gas interaction. B) Image of the plasma channel ( $\sim 200\text{-}300\ \mu\text{m}$  diameter, 10 mm length) created during the laser-gas interaction.

The case of a solid target interacting with the laser is presented in Figure 4 which displays pictures of a thin foil positioned at the laser pulse focus, captured both 20 ps before the interaction of the 1 PW pulse with the target and 200 ps afterward. These measurements were performed during the experimental campaign at ELI-NP for proton acceleration, which took place in the C3 interaction chamber of the E5 experimental area. The target consisted of a  $20\ \mu\text{m}$  thick Aluminum foil and was mounted on a specially designed holder, which allowed the visualization of the target expansion during irradiation. The plasma plume expansion induced by the main laser beam is clearly visible in the image taken 200 ps post-interaction in Fig. 4B where the direction of the laser is indicated by the apex of the cone. We observed the formation of two plasma plumes, one facing the laser beam and the other one at the target's rear side. The opaque feature of the plasma is directly related to its density value, which appears to be larger or close to the critical level  $n_c = 1.7 \times 10^{21}\text{cm}^{-3}$  above which the 800 nm laser light is absorbed. Acceleration of particles takes place on both sides of the target foil. The electrons from the ionized target front surface are driven by the laser pulse to the rear target surface where create a space charge with an intense electric field of the order of  $\text{MV}/\mu\text{m}$  near the surface. The protons and ions are accelerated to high energies by this field in the target normal direction, as described by the TNSA (Target Normal Sheath Acceleration) mechanism [17]. The energy spectra of proton and ions are related to the features of the plasma formed by the target ionization and depend on several factors as for instance target thickness, density, surface structure, material, etc. [18]. Also, the energy of accelerated particles,  $E_p$ , scales as  $E_p \sim I_L^{1/2}$ , where  $I_L$  is the laser peak intensity in the focal spot.

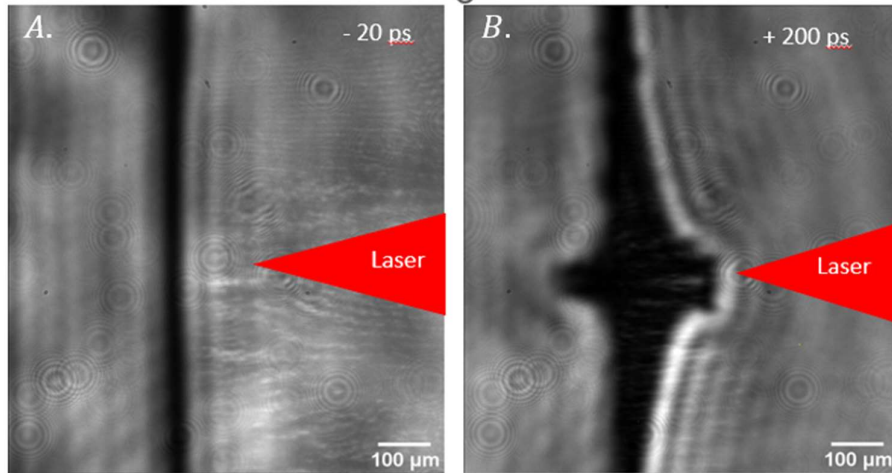


Fig. 4. – Shadowgraphy from the side of the Aluminium thin foil target at different moments, A. 20 ps prior to interacting with the main laser pulse (i.e., -20 ps) and B. after the interaction with the main laser pulse at +200 ps.

#### 4. CONCLUSIONS

The techniques of Shadowgraphy and Interferometry in Quadruple Wavefront Lateral Shearing were used during the commissioning experiments of the 1 PW laser beam with solid and gas targets, in the E5 experimental area. These imaging diagnostics were applied to optimize the configuration of both solid and gas targets, as well as to fine-tune the focus spot position and other parameters of the 1 PW laser beam. The commissioning experiments focused on the acceleration of protons to tens of MeV energy from solid targets in the C3 interaction chamber and on the acceleration of electrons to over 1 GeV with gas targets in the C1 interaction chamber. Together, the two experimental methods provide complementary imaging and diagnostic information for laser-plasma interaction at ultrafast time scales.

**Acknowledgements.** This work was funded through the Extreme Light Infrastructure Nuclear Physics (ELI-NP) Project, Phases I (475/12.12.2012) and II (1/07.07.2016), co-financed by the Romanian Government and the European Union via the European Regional Development Fund. We extend our gratitude to the Romanian Ministry of Research, Innovation, and Digitalization for supporting the Program Nucleu projects PN 23210105 and PN 19060105. Access to the ELI-NP facility was made possible through IOSIN funds for research infrastructures of national interest, provided by the Romanian Ministry of Research, Innovation, and Digitalization.

## REFERENCES

1. A. Măgureanu *et al.*, "Plasma imaging diagnostics for high-power lasers experiments", Internal report in ELI-NP Annual Report 2020-2021 (2022), [www.eli-np.ro/documents/ELI-NP-Annual\\_Report-2020-2021.pdf](http://www.eli-np.ro/documents/ELI-NP-Annual_Report-2020-2021.pdf).
2. K. A. Tanaka *et al.*, "Current status and highlights of the ELI-NP research program," *Matter and Radiation at Extremes*, vol **5**, 024402 (2020).
3. D. Doria *et al.*, "Overview of ELI-NP status and laser commissioning experiments with 1 PW and 10 PW class-lasers", *Journal of Instrumentation* C09053, vol **15** (2020).
4. J. F. Ong *et al.*, "Nuclear photonics: Laser-driven nuclear physics", *IOP Conf. Series: Mater. Sci. Eng.* **1285** 012003 (2023).
5. M. C. Downer *et al.*, "Diagnostics for plasma-based electron accelerators", *Rev. Mod. Phys.* vol **90**, 035002 (2018).
6. S. S. Harilal *et al.*, "Optical diagnostics of laser-produced plasmas", *Rev. Mod. Phys.* vol. **94**, 035002 (2022).
7. A. Boné *et al.*, "Quantitative shadowgraphy for laser-plasma interactions", *J. Phys. D: Appl. Phys.* **49** 155204 (2016)
8. G. R. Plateau *et al.*, "Wavefront-sensor-based electron density measurements for laser-plasma accelerator", *Review of Scientific Instruments*, vol **81**, 033108 (2010)
9. A. Sävert *et al.*, "Direct Observation of the Injection Dynamics of a Laser Wakefield Accelerator Using Few-Femtosecond Shadowgraphy", *Physical Review Letters*, vol. **115**, pp. 055002/1-5 (2015)
10. M. O. Cernaianu *et al.*, "Commissioning of the 1 PW experimental area at ELI-NP using a short focal length parabolic mirror for proton acceleration", *Matter Radiat. Extremes*, vol **10**, 027204 (2025)
11. M. B. Schwab *et al.*, "Few-cycle optical probe-pulse for investigation of relativistic laser-plasma". *Applied Physics Letters*, vol. **103**, pp. 191118 (1-5) (2013)
12. F. Lureau *et al.*, "High-energy hybrid femtosecond laser system demonstrating  $2 \times 10$  PW capability", *High Power Laser Science and Engineering*, vol **8**, p. e43 (2020).
13. R. A. Negres *et al.*, "40-fs broadband low dispersion mirror thin film damage competition"; *Proceedings Volume 10014, Laser-Induced Damage in Optical Materials 2016*, 100140E (2016).
14. J. Primot *et al.*, "Achromatic three-wave (or more) lateral shearing interferometer," *Journal of the Optical Society of America A*, vol. **12**, 2679-2685 (1995)
15. S. Velghe *et al.*, "Advanced wave-front sensing by quadri-wave lateral shearing interferometry," *Proc. SPIE 6292, Interferometry XIII: Techniques and Analysis*, 62920E (2006)
16. G. Baffou, "Quantitative phase microscopy using quadriwave lateral shearing interferometry (QLSI): principle, terminology, algorithm and grating shadow description", *Journal of Physics D: Applied Physics*, vol **54**, pp.294002 (2021).
17. M. Roth, M. Schollmeier, "Ion Acceleration—Target normal Sheath Acceleration. In: B Holzer, editor. *Proceedings of the CAS-CERN Accelerator School: Plasma Wake Acceleration*; 23–29 November 2014; Geneva, Switzerland. SPIE (2016).
18. A. Măgureanu *et al.*, "Target characteristics used in laser-plasma acceleration of protons based on the TNSA mechanism", *Front. Phys.* **10**, 727718 (2022).